Peptidoglycan layer and disruption processes in *Bacillus subtilis* cells visualized using quick-freeze, deep-etch electron microscopy

Isil Tulum[a,b,1], Yuhei O Tahara[a,b,1], Makoto Miyata[a,b,2]

[a] Graduate School of Science, Osaka City University, Osaka, 558-8585, Japan. [b] The OCU Advanced Research Institute for Natural Science and Technology (OCARINA), Osaka City University, Osaka, 558-8585, Japan.

Abstract

Peptidoglycan, which is the main component of the bacterial cell wall, is a heterogeneous polymer of glycan strands crosslinked with short peptides and is synthesized in cooperation with the cell division cycle. Although it plays a critical role in bacterial survival, its architecture is not well understood. Herein, we visualized the architecture of the peptidoglycan surface in *Bacillus subtilis* at the nanometer resolution, using quick-freeze, deep-etch electron microscopy. Filamentous structures were observed on the entire surface of the cell, where filaments about 11-nm wide formed concentric circles on cell poles, filaments about 13-nm wide formed a circumferential mesh-like structure on the cylindrical part, and a "piecrust" structure was observed at the boundary. When growing cells were treated with lysozyme, the entire cell mass migrated to one side and came out from the cell envelope. Fluorescence labeling showed that lysozyme preferentially bound to a cell pole and cell division site, where the peptidoglycan synthesis was not complete. Ruffling of surface structures was observed during electron microscopy. When cells were treated with penicillin, the cell mass came out from a cleft around the cell division site. Outward curvature of the protoplast at the cleft seen using electron microscopy suggested that turgor pressure was applied as the peptidoglycan was not damaged at other positions. When muropeptides were depleted, surface filaments were lost while the rod shape of the cell was maintained. These changes can be explained on the basis of the working points of the chemical structure of peptidoglycan.

Keywords: Lysozyme, Penicillin, Piecrust, L-form, MurE, Turgor

Significance Statement

Bacteria, the major inhabitants of the Earth, are in a constant battle to outlast their competitors in the environment and the immune system of host organisms. Most bacterial cells are surrounded by a rigid shield called the "peptidoglycan layer," which protects them from chemical agents, including lytic enzymes and antibiotics, that are produced by their competitors. In this study, we visualized this layer that protects the bacteria from these agents using quick-freeze, deep-etch electron microscopy, a special technique that can be used to visualize

detailed structures on bacterial surfaces in high spatial and time resolutions.

Introduction

Peptidoglycan is an essential component of the bacterial cell wall that is found on the outside of the cytoplasmic membrane of almost all bacterial cells except the class *Mollicutes*. This polymer provides strength, rigidity, and shape stability by maintaining turgor pressure (1-4). In peptidoglycan, the glycan strands comprise alternating β-1,4-linked *N*-acetylglucosamine (GlcNAc) and *N*-acetylmuramic acid (MurNAc), and the peptide stems are covalently linked to the glycan strands with an amide bond to the carboxyl carbon of the MurNAc. The peptidoglycan layer is also the site of action for antimicrobial agents. Lysozyme, an antimicrobial enzyme critical in animal host defense, is one of the most abundant proteins present on the mucosal surfaces and in body secretions, such as saliva and tears (5, 6). The epithelial cells secrete lysozyme to protect the host's mucosal surfaces from infectious bacteria. Lysozyme is also present in white blood cells, especially in granules of phagocytes, where it helps in the elimination of infectious bacteria within phagolysosomes. The underlying mechanism of action of lysozyme involves breaking the bond between GlcNAc and MurNAc (muramidase activity) leading to the degradation of peptidoglycan. On the other hand, fungi and bacteria produce secondary metabolites in defense against predators and competitors (7, 8). A well-known group of secondary metabolites is beta-lactams, a broad class of antibiotics that include penicillin derivatives, cephalosporins, monobactams, and carbapenems. Beta-lactams inhibit peptidoglycan synthesis by covalently binding to the active site of transpeptidases, known as penicillin-binding proteins (PBPs), and cause changes in bacterial cell shape and lead to cell lysis.

This property makes peptidoglycan a vitally important target of beta-lactam antibiotics. Therefore, peptidoglycan architecture and the processes that are used to disrupt it are valuable to understand the survival strategies of bacteria and to control pathogenic bacteria. However, the architecture of peptidoglycan is not well understood, because the structure is featured with low density, high flexibility, and is multilayered, which are characteristics that make it unsuitable to be observed using transmission electron microscopy (EM)(2, 9-13).

Quick-freeze, deep-etch replica EM was introduced in order to visualize synaptic transmission processes in 1979, and it has emerged as a useful tool that can be applied for the visualization of many other biological phenomena (14). It is an advanced technology that is used to visualize biological specimens in an active state as a shot image, with spatial resolution of the nanometer order and time resolution of sub milliseconds, because the specimen is frozen quickly by pressing it against a metal block chilled with liquid helium or liquid nitrogen and shadowed by platinum with high contrast. Therefore, this method has great advantages when used to visualize low density and flexible structures in comparison to other methods of transmission EM.

Bacillus subtilis is a rod-shaped, Gram-positive, non-pathogenic bacterium that belongs to the phylum *Firmicutes* (1). The genus *Bacillus* also includes human pathogens such as *Bacillus anthracis* and *Bacillus cereus* (15) and is related to the genus *Clostridium*. Therefore, *B. subtilis* can be an attractive model for the clarification of the architecture and the roles of the cell wall. In this study, the detailed structures of the peptidoglycan layer and its disruption processes in *B. subtilis* were analyzed using the quick-freeze, deep-etch EM and optical microscopy.

Results

Surface structure of *Bacillus subtilis*

To visualize the structure of the peptidoglycan layer, *B. subtilis* was observed for the first time by the quick-freeze, deep-etch EM. Cells in exponential growth phase were collected by centrifugation and placed on glass, frozen, fractured, deeply etched, shadowed with platinum, and then the platinum replicas were recovered and observed. The shape and dimensions of the cells were consistent with the images of living cells obtained by optical microscopy (Fig. 1A, B). Filamentous structures were clearly observed on the cell surface and can be distinguished between the cell pole and the cylindrical part on the rod-shaped cells (Fig. 1C, D and Movie S1). The thick filaments 12.7 ± 0.4 nm wide were aligned in partial circumferential manner on the cylindrical part. The filament widths were measured based on the image profile (Fig. S1). The thin filaments 10.9 ± 0.3 nm wide were concentrically arranged around the both poles with a

pitch of 11.3 ± 0.4 nm (Fig. 1E, F).

On elongated cells prior to cell division, invagination was observed at the central position of the axis, and an obvious boundary was found between the cylindrical part and the surface of the invagination (Fig. 1G). Obvious filamentous structures were not found on the surface of the invagination. A wall 24.8 ± 1.6 nm wide was observed between the surface of the invagination and the cylindrical part (Fig. 1G). This small wall was also found in cells after division (Fig. 1H), but not in isolated single cells (Fig. 1D).

Peptidoglycan disruption by lysozyme

Next, we examined how the peptidoglycan layer is disrupted by lysozyme. We added lysozyme from the egg white to growing cells, and observed the changes occurring on the cell structures by phase-contrast optical microscopy (Fig. 2A). The effects of lysozyme on *B. subtilis* cells were consistent with previous reports, although we traced the changes in more detail (5, 16, 17). In the present observation, the cell mass started to detach from the envelope structure around 30 minutes after the addition of lysozyme and moved to one side over time. Finally, all the mass was localized as a sphere at one side of the cell envelope. After a 60 minute treatment, 100% of the cells (n = 72) were converted to protoplast.

In order to locate the sites where lysozyme works on the cell in this process, we labeled lysozyme fluorescently and traced where it attached (Fig. 2B). After 10 minutes , the labeled lysozyme bound to the whole cell surface but preferentially bound to the division site and a cell pole. The changes in lysozyme localization over time were traced through live imaging (Fig. 2C). The signal found at a pole decreased with time and disappeared at 40 minutes. The signal on parts other than the cell poles remained for 40 minutes, and then it moved to one side. The disappearance of lysozyme signal should suggest the dissociation of lysozyme from envelope, caused by the complete digestion of the target sites on the peptidoglycan layer.

Next, we observed the structural changes on cell surface at high resolution using the quick-freeze, deep-etch EM (Fig. 2D□E). At 20 minutes after the addition of lysozyme, ruffling of the surface structure was observed around a cell

pole, which is probably corresponding to the area to which lysozyme bound on the cell. The peptidoglycan layer should detach from the cell partly by the degradation of the sugar chain. At 60 minutes, the ruffling parts became restrictive, which is consistent with the observation that the area of lysozyme binding became restrictive in the fluorescence microscopy. Instead of ruffling, we found coarse patterns on the cylindrical part of cells and spherical structures with a smooth surface, suggesting that lysozyme moved and digested the peptidoglycan at the cylindrical parts.

Peptidoglycan disruption by penicillin

The process of peptidoglycan disruption by the effect of penicillin was examined (Fig. 3). Beginning 30 minutes after the addition of 100 µg/mL Penicillin G (PenG) to the growing culture, a less dense and flexible structure was observed to project from a side position on a cell under optical microscopy (Fig. 3A). At 120 minutes, 89% of the cells (n = 172) were released from the peripheral structure probably as a protoplast.

Next, the cells damaged by PenG treatment for 120 minutes were observed by the quick-freeze, deep-etch EM (Fig. 3B, C). The images were defined by eutectics, which should be caused by the cytosol eluted from damaged cells, because generally some ions and polymers form eutectics in the quick-freeze, deep-etch EM (18). The cell images showed various stages of the process by which a protoplast comes out from the cell envelope. In many cases, the cytoplasm came out from the central position of the cell where the cell division should be scheduled (Fig. 3C). Unlike the effect of lysozyme, the cytoplasm in the early stage of cell disruption seemed to be subjected to strong turgor, because the protoplasts coming through the cleft had some outward curvature.

Peptidoglycan disruption by *murE* operon repression

The repression of the *murE* operon ceases supplying muropeptides, induces the gentle degradation of the peptidoglycan layer, and then results in the transfer of *B. subtilis* cells into L-form (19, 20). This process was visualized by phase-contrast optical microscopy (Fig. 4A). When the *murE* operon was repressed for 80 minutes, the cell morphology was disturbed mostly around cell

poles, featured by a tapered pole, and the detachment of cell mass from the pole. Time lapse imaging of cells showed that these two features occurred in a sequential manner. In those cells, finally the cell became spherical, which may proliferate as L-form. These processes agree with those previously reported (19, 20). Next, we visualized the cells by the quick-freeze, deep-etch EM. Irregular cell shapes were obvious under this method, including asymmetric cell division, tapered cell pole (Fig. 4B), and spherical extension at a cell pole (Fig. 4C, left). The filaments on the cell surfaces were unclear compared to the original cells or totally lacking (Fig. 4C, left and middle). On the spherical cells, no filaments were found on the surface, supporting our assumption that the filaments observed in the quick-freeze, deep-etch EM are derived from the peptidoglycan layer (Fig. 4C, right).

Discussion

Visualization of peptidoglycan layer by quick-freeze, deep-etch EM

The images obtained by the quick-freeze, deep-etch EM may appear like those from Scanning Electron Microscopy (SEM), but they are featured by 10 folds higher spatial resolution and sub-millisecond time resolution. This method should be very efficient for research of microorganisms whose interaction with the environment on their surface is critical for many activities (14, 21, 22). In the present study, the quick-freeze, deep-etch EM was applied to the visualization of the peptidoglycan and its disruption process, for the first time. The results showed the details of filamentous structures in nanometer resolution and its change with time resolution, as expected.

In normally growing cells, the alignments of the peptidoglycan filaments were clearly distinguished between the poles and the cylindrical part (Figs. 1 and 5A left). This was consistent with the knowledge from molecular biology that peptidoglycan synthase is localized by MreB when cells are elongating and the synthase is localized at the division site by FtsZ during cell division (23, 24). The concentric pattern in the pole is considered to be common to the structure previously observed by a related method, the freeze fracture of fixed cells of *Staphylococcus* (25). Atomic Force Microscopy (AFM) of the peptidoglycan showed circular pattern for *B. subtilis* (12) and also for *Lactococcus lactis (11)*.

The circular pattern observed in the present study may be general in *Firmicute* bacterial species, although the appearance depends on the visualizing methods. A small wall structure was seen at the boundary between the surfaces of the invaginating part and the cylindrical part (Fig. 1G, H). This structure should correspond to a structure named “wall band” observed in sectioned EM images (26, 27). A similar structure is known as “piecrust” in SEM observation of *Staphylococcus aureus* (25), although it has not been observed in SEM images of *B. subtilis* (2). In previous observations of *B. subtilis* using SEM, the low resolution and chemical fixation processes interfered with the visualization of the piecrusts. The filament pattern observed on the cylindrical part is a circumferential mesh-like structure similar to the pattern observed for the isolated peptidoglycan layer of *Escherichia coli* using AFM, although the filament widths are different (9). Perhaps, the filaments in the cylindrical part may be aligned roughly in a circumferential way, generally in rod shaped bacteria (10, 12, 13).

Based on the observation here, we can suggest a scheme for cell surface structures in cell division cycles (Fig. 5A left).

Lysozyme starts from new pole and division site

In the present study, the disruption process of the peptidoglycan layer was visualized for each of the three factors with different working points (Fig. 5A right, B). In the process, lysozyme preferentially bound to a cell pole and a cell division site (Fig. 2B). Probably, the newly synthesized peptidoglycan has many gaps, which lysozyme molecules can access easily. The tracking of lysozyme showed that it detached from the initially bound position earlier than it did the other parts, suggesting that the peptidoglycan digestion was completed at the cell pole (Fig. 2C). Even when pathogenic or parasitic bacteria invade the host, the division site and the new pole is preferentially attacked by lysozyme. We focused on *B. subtilis* inhabiting the environment in the present study, but the process by which lysozyme attacks pathogenic or parasitic bacteria should also be very interesting.

Quick-freeze, deep-etch EM showed that the action of lysozyme loosens the peptidoglycan. As lysozyme cleaves carbohydrate chains that mainly form the

filaments of the peptidoglycan layer (Fig. 5B)(6), the peptidoglycan layer separates from the cell surface (Fig. 2E). This damage on the entire peptidoglycan layer is as effective as the protection system that is involved in the resistance against invasion by pathogenic or parasitic bacteria.

Turgor by penicillin treatment

In the early stage of cell disruption by PenG, large turgor appeared to be applied to the cytoplasm at the cell division site from the cell inside, because the cell membrane at a cleft of the cell envelope showed curvature to outside (Figs. 3C and 5A right). In the process by lysozyme, such turgor was not observed. This difference can be explained by the disruption mechanisms (Fig. 5B)(5, 6, 28). As PenG inhibits only *de novo* crosslinking of peptidoglycan, the maturated parts of the peptidoglycan layer apply turgor to the cell. However, the damages by lysozyme disrupt whole parts of cell envelope.

Change in surface pattern after *murE* operon repression

When the supply of muropeptide was stopped, the cell shape was disturbed around the cell pole (Figs. 4 and 5A right). At that time, the features of the pattern on the surface were also lost. Since the peptidoglycan layer of *B. subtilis* is 20–40 nm thick, insertion of newly synthesized filaments into the peptidoglycan layer through muropeptide supply is thought to occur on the side close to the membrane (29, 30). If it is true, the influence on the surface pattern of the muropeptide depletion should occur in the final stage of morphological change. In fact, a noticeable change in pattern was observed when the cells were still maintaining the rod shape (Fig. 4C). This may suggest that there is fluidity in the existing peptidoglycan filaments (30, 31).

Materials and Methods

Bacterial strains and media. *Bacillus subtilis* 168 CA and LR2, a strain inducible for L-form derived from *B. subtilis* 168 CA (5, 32) were used. Nutrient agar (NA, Oxoid) was used for routine selection and maintenance of *B. subtilis* 168 CA. Luria–Bertani (LB), nutrient broth (NB, Oxoid), and SMM-defined minimal medium (Spizizen) containing 0.5% xylose or 1 mM isopropyl

β-D-1-thiogalactopyranoside (IPTG) were used when required.

Treatment of cells. Cultured cells around optical density (OD) at 0.2 in 600 nm wavelength, a middle exponential stage, were collected by centrifugation at 8,000 × *g*, room temperature (RT) for 3 minutes. For lysozyme treatment, the cells were suspended in phosphate-buffered saline consisting of 75 mM sodium phosphate (pH 7.3) and 68 mM NaCl to be the original cell density. Lysozyme was added to the cell suspension at final concentration of 0.1 mg/mL and kept at 37°C without shaking. For PenG treatment, cultured cells were collected and suspended in a new medium at the original cell density. PenG was added at the final concentration of 0.1 mg/mL and kept at 37°C with shaking. To induce the L-form transition, 2 × MSM osmoprotective medium (40 mM $MgCl_2$, 1 M sucrose and 40 mM maleic acid, pH 7.0) was mixed with the same volume of 2 × NB or 2 × NA. L-form liquid cultivation was done in NB/MSM at 30°C without shaking (32). Lysozyme hydrochloride, from egg white (Wako Pure Chemical Industries, Osaka, Japan) was labeled with DyLight 488 NHS Ester (Thermo Fisher Scientific, Rockford, IL), according to the instruction.

Optical microscopy. The cells were inserted into a tunnel chamber with a 5-mm interior width, a 22-mm length, and an 86-μm wall thickness (33). The tunnel chamber was constructed with a coverslip and a glass slide and assembled with double-sided tape. Fluorescence microscopy was performed with a BX51 fluorescence microscope equipped with a YFP filter unit (U-MYFPHQ) and a phase-contrast setup (Olympus, Tokyo, Japan). Images were captured with a WAT-120NRC charge-coupled-device (CCD) camera (Watec, Yamagata, Japan) and analyzed using ImageJ 1.52.

Quick-freeze, deep-etch EM. The cells were collected by centrifugation and suspended in a buffer consisting of 1 mM $MgCl_2$ and 0.1 mg/mL DNase I to be 20 folds higher cell density. The cell suspension was mixed with a slurry that included mica flakes, placed on a rabbit lung slab, and frozen by a CryoPress (Valiant Instruments, St. Louis, MO) cooled by liquid helium. The specimens were fractured and etched for 15 minutes at -104°C, in a JFDV freeze-etching

device (JEOL Ltd, Akishima, Japan). The exposed cells were rotary-shadowed by platinum at an angle of 20 degree to be 2 nm in thickness and backed with carbon. Replicas were floated off on full-strength hydrofluoric acid, rinsed in water, cleaned with a commercial bleach, rinsed in water, and picked up onto copper grids as described (34). Replica specimens were observed by a JEM-1010 transmission electron microscope (JEOL, Tokyo, Japan) at 80 kV equipped with a FastScan-F214 (T) CCD camera (TVIPS, Gauting, Germany). For tomography, cell replicas were observed by Talos F200C G2 (Thermo fisher Scientific, Waltham, MA, USA) at 200 kV, and image sets were acquired every degree of angle for 96 steps, by a complementary metal–oxide-semiconductor (CMOS) camera (Ceta camera, FEI). The images were analyzed by ImageJ.

Acknowledgements

We appreciate the helpful input from Eisaku Katayama at Osaka City University and Daisuke Shiomi at Rikkyo University, gift of *Bacillus subtilis* strains from Yoshikazu Kawai at Newcastle University, and technical support from Junko Shiomi at Osaka City University. The application of quick-freeze, deep-etch EM technique to microbiology was developed as the general supporting project for the Grant-in-Aid for Scientific Research on Innovative Areas “Harmonized Supramolecular Motility Machinery and Its Diversity” (25117501) directed by MM. This work was supported by a Grant-in-Aid for Scientific Research on the Innovative Area “Harmonized Supramolecular Motility Machinery and Its Diversity” (MEXT KAKENHI Grant Number 24117002) and by Grant-in-Aids for Scientific Research (B) and (A) (MEXT KAKENHI Grant Numbers 24390107 and 17H01544) to MM.

Footnotes

[1]I.T. and Y.O.T. contributed equally to this work.

[2] To whom correspondence should be addressed. Email: miyata@sci.osaka-cu.ac.jp.

Author contributions: All authors contributed to the research design, analyzing data and writing the paper; I.T. and Y.O.T. performed the experiments. The authors declare no conflict of interest.

Reference

1. Errington J (2013) L-form bacteria, cell walls and the origins of life. *Open Biol* 3(1):120143.
2. Turner RD, Vollmer W, & Foster SJ (2014) Different walls for rods and balls: the diversity of peptidoglycan. *Mol Microbiol* 91(5):862-874.
3. Erickson HP (2017) How bacterial cell division might cheat turgor pressure - a unified mechanism of septal division in Gram-positive and Gram-negative bacteria. *Bioessays* 39(8).
4. Osawa M & Erickson HP (2018) Turgor pressure and possible constriction mechanisms in bacterial division. *Front Microbiol* 9:111.
5. Kawai Y, Mickiewicz K, & Errington J (2018) Lysozyme counteracts beta-lactam antibiotics by promoting the emergence of L-form bacteria. *Cell* 172(5):1038-1049 e1010.
6. Ragland SA & Criss AK (2017) From bacterial killing to immune modulation: Recent insights into the functions of lysozyme. *PLoS Pathog* 13(9):e1006512.
7. Stulberg ER, *et al.* (2016) Genomic and secondary metabolite analyses of *Streptomyces* sp. 2AW provide insight into the evolution of the cycloheximide pathway. *Front Microbiol* 7:573.
8. Kunzler M (2018) How fungi defend themselves against microbial competitors and animal predators. *PLoS Pathog* 14(9):e1007184.
9. Turner RD, Mesnage S, Hobbs JK, & Foster SJ (2018) Molecular imaging of glycan chains couples cell-wall polysaccharide architecture to bacterial cell morphology. *Nat Commun* 9(1):1263.
10. Beeby M, Gumbart JC, Roux B, & Jensen GJ (2013) Architecture and assembly of the Gram-positive cell wall. *Mol Microbiol* 88(4):664-672.
11. Andre G, *et al.* (2010) Imaging the nanoscale organization of peptidoglycan in living Lactococcus lactis cells. *Nat Commun* 1:27.
12. Hayhurst EJ, Kailas L, Hobbs JK, & Foster SJ (2008) Cell wall peptidoglycan architecture in *Bacillus subtilis*. *Proc Natl Acad Sci U S A* 105(38):14603-14608.
13. Gan L, Chen S, & Jensen GJ (2008) Molecular organization of Gram-negative peptidoglycan. *Proc Natl Acad Sci U S A* 105(48):18953-18957.
14. Heuser JE (2011) The origins and evolution of freeze-etch electron microscopy. *J Electron Microsc (Tokyo)* 60 Suppl 1:S3-29.
15. Swick MC, Koehler TM, & Driks A (2016) Surviving between hosts: sporulation and transmission. *Microbiol Spectr* 4(4).
16. Weibull C (1953) The isolation of protoplasts from *Bacillus megaterium* by controlled treatment with lysozyme. *J Bacteriol* 66(6):688-695.
17. Muchova K, Wilkinson AJ, & Barak I (2011) Changes of lipid domains in Bacillus subtilis cells with disrupted cell wall peptidoglycan. *FEMS Microbiol Lett* 325(1):92-98.
18. Miller KR, Prescott CS, Jacobs TL, & Lassignal NL (1983) Artifacts associated with quick-freezing and freeze-drying. *J Ultrastruct Res* 82(2):123-133.
19. Dominguez-Cuevas P, Mercier R, Leaver M, Kawai Y, & Errington J (2012) The rod to L-form

transition of Bacillus subtilis is limited by a requirement for the protoplast to escape from the cell wall sacculus. *Mol Microbiol* 83(1):52-66.

20. Leaver M, Dominguez-Cuevas P, Coxhead JM, Daniel RA, & Errington J (2009) Life without a wall or division machine in *Bacillus subtilis*. *Nature* 457(7231):849-853.

21. Hung C, *et al.* (2013) *Escherichia coli* biofilms have an organized and complex extracellular matrix structure. *MBio* 4(5):e00645-00613.

22. Yoshida S, *et al.* (2006) Microtubule-severing activity of Shigella is pivotal for intercellular spreading. *Science* 314(5801):985-989.

23. Cabeen MT & Jacobs-Wagner C (2007) Skin and bones: the bacterial cytoskeleton, cell wall, and cell morphogenesis. *J Cell Biol* 179(3):381-387.

24. Typas A, Banzhaf M, Gross CA, & Vollmer W (2011) From the regulation of peptidoglycan synthesis to bacterial growth and morphology. *Nat Rev Microbiol* 10(2):123-136.

25. Amako K, Umeda A, & Murata K (1982) Arrangement of peptidoglycan in the cell wall of *Staphylococcus* spp. *J Bacteriol* 150(2):844-850.

26. Burdett ID (1979) Electron microscope study of the rod-to-coccus shape change in a temperature-sensitive rod- mutant of *Bacillus subtilis*. *J Bacteriol* 137(3):1395-1405.

27. Burdett ID & Higgins ML (1978) Study of pole assembly in Bacillus subtilis by computer reconstruction of septal growth zones seen in central, longitudinal thin sections of cells. *J Bacteriol* 133(2):959-971.

28. Monahan LG, *et al.* (2014) Rapid conversion of *Pseudomonas aeruginosa* to a spherical cell morphotype facilitates tolerance to carbapenems and penicillins but increases susceptibility to antimicrobial peptides. *Antimicrob Agents Chemother* 58(4):1956-1962.

29. Kim SJ, Chang J, & Singh M (2015) Peptidoglycan architecture of Gram-positive bacteria by solid-state NMR. *Biochim Biophys Acta* 1848(1 Pt B):350-362.

30. Zhao H, Patel V, Helmann JD, & Dorr T (2017) Don't let sleeping dogmas lie: new views of peptidoglycan synthesis and its regulation. *Mol Microbiol* 106(6):847-860.

31. Shi H, Bratton BP, Gitai Z, & Huang KC (2018) How to build a bacterial cell: MreB as the foreman of *E. coli* construction. *Cell* 172(6):1294-1305.

32. Mercier R, Kawai Y, & Errington J (2013) Excess membrane synthesis drives a primitive mode of cell proliferation. *Cell* 152(5):997-1007.

33. Kasai T, Hamaguchi T, & Miyata M (2015) Gliding motility of *Mycoplasma mobile* on uniform oligosaccharides. *J Bacteriol* 197(18):2952-2957.

34. Miyata M & Petersen JD (2004) Spike structure at the interface between gliding *Mycoplasma mobile* cells and glass surfaces visualized by rapid-freeze-and-fracture electron microscopy. *J Bacteriol* 186(13):4382-4386.

LEGENDS

Movie S1. Tomogram of isolated cell for 96 degrees. The cylindrical and cell pole parts are colored differently in a still image at zero angle.

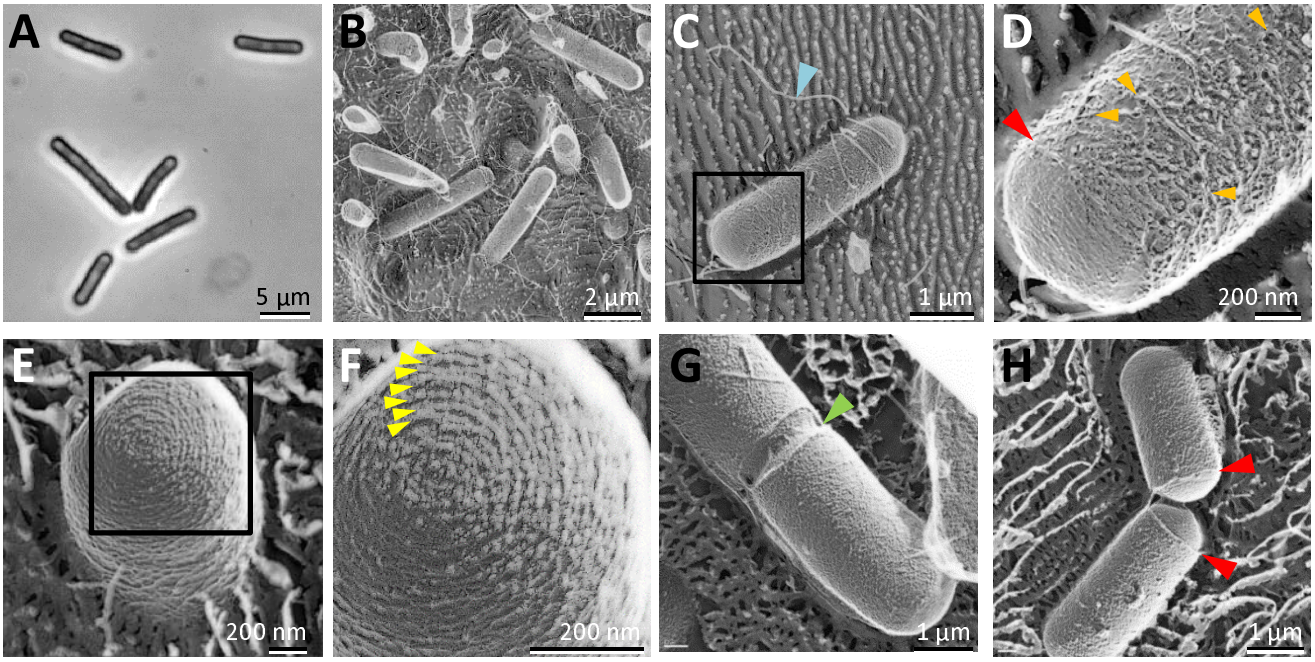

Fig. 1. Surface structures of *Bacillus subtilis* 168 CA strain cells visualized by quick-freeze, deep-etch EM. **A)** Phase-contrast optical microscopy of cells. **B)** Field image of cells. **C-H)** Magnified cell images. **C**) Side view. A flagellum is marked by a blue triangle. A boxed area is magnified in (D). **D)** Magnified cell surface image. Filaments on the cylindrical part are marked by orange triangles. The boundary between the cylindrical and pole parts are marked by a red triangle. **E**) Pole view. A boxed area is magnified in (F). **F)** Magnified pole surface image. Concentric circles are marked by yellow triangles. **G)** Dividing cell. The invagination is marked by a green triangle. **H)** Daughter cells probably just after cell division. Piecrust structures are marked by red triangles.

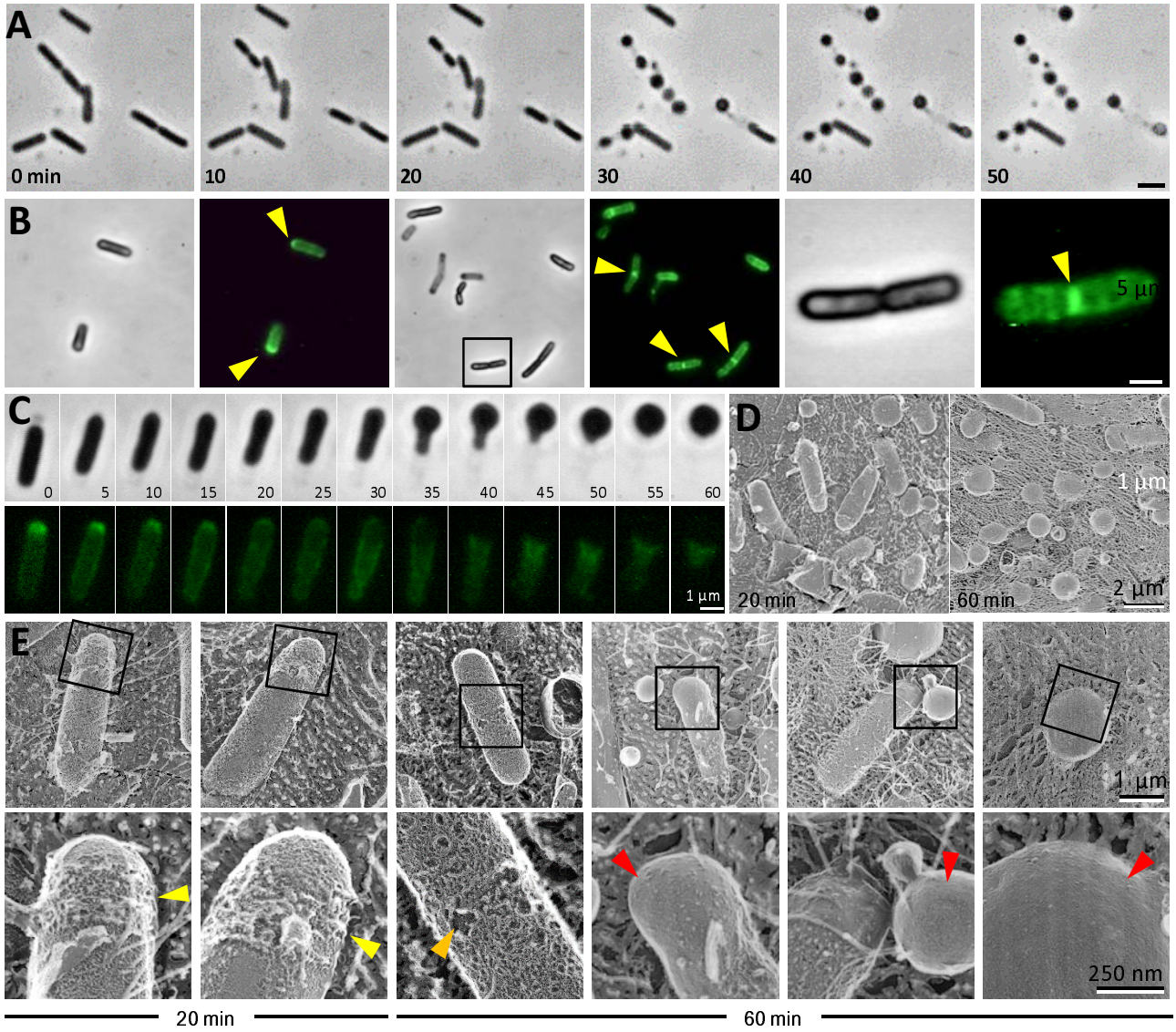

Fig. 2. Damages on cell structure by lysozyme. **A)** Phase-contrast microscopic images after addition of lysozyme taken with 10 minutes intervals. **B)** Localization of fluorescently labeled lysozyme on cell. Fluorescence of labeled lysozyme was visualized at 10 minutes after the addition. Phase-contrast and fluorescence images are shown as the left and the right panels, respectively in each of three image sets. A boxed cell in the middle-paired panels is magnified in the right panel set. The signals were found preferentially at a pole and the division site as marked by yellow triangles. **C)** Phase-contrast and fluorescence images of single cell treated by labeled lysozyme taken with 5-minutes intervals. **D)** Field image of cells treated with lysozyme for 20 and 60 minutes taken by the quick-freeze, deep-etch EM. The mica surface is covered by eutectics appearing as thin filaments. **E)** Quick-freeze, deep-etch EM images of cells treated with lysozyme for 20 and 60 minutes, as shown in the bottom. The focused regions boxed in the upper panels are magnified in the lower panels. Ruffling, coarse pattern and smooth surfaces are marked by yellow, orange and red triangles, respectively.

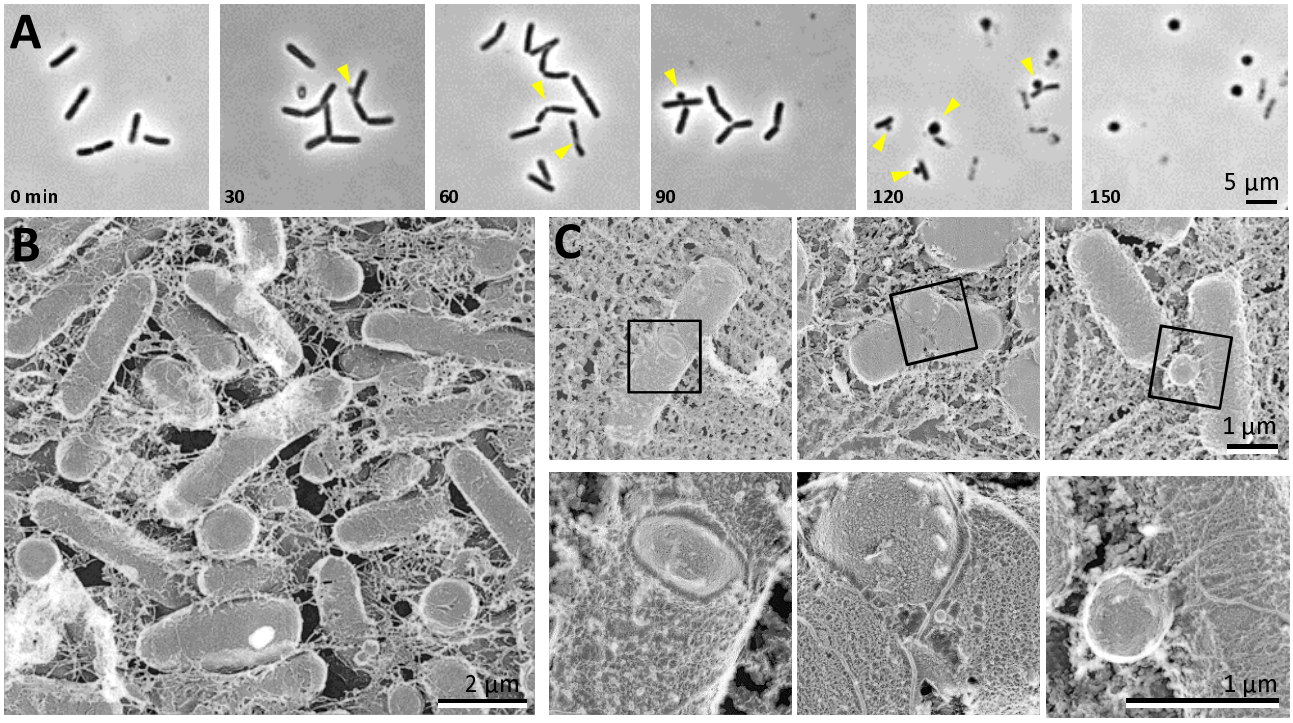

Fig. 3. Damages on cell structure by PenG. **A)** Phase-contrast microscopic images after addition of PenG taken at 30-minutes intervals. **B, C)** Quick-freeze, deep-etch EM images of cells treated with PenG for 120 minutes. **B**) Field image. **C**) Magnified cell images. The boxed regions in the upper panels are magnified more in the lower panels.

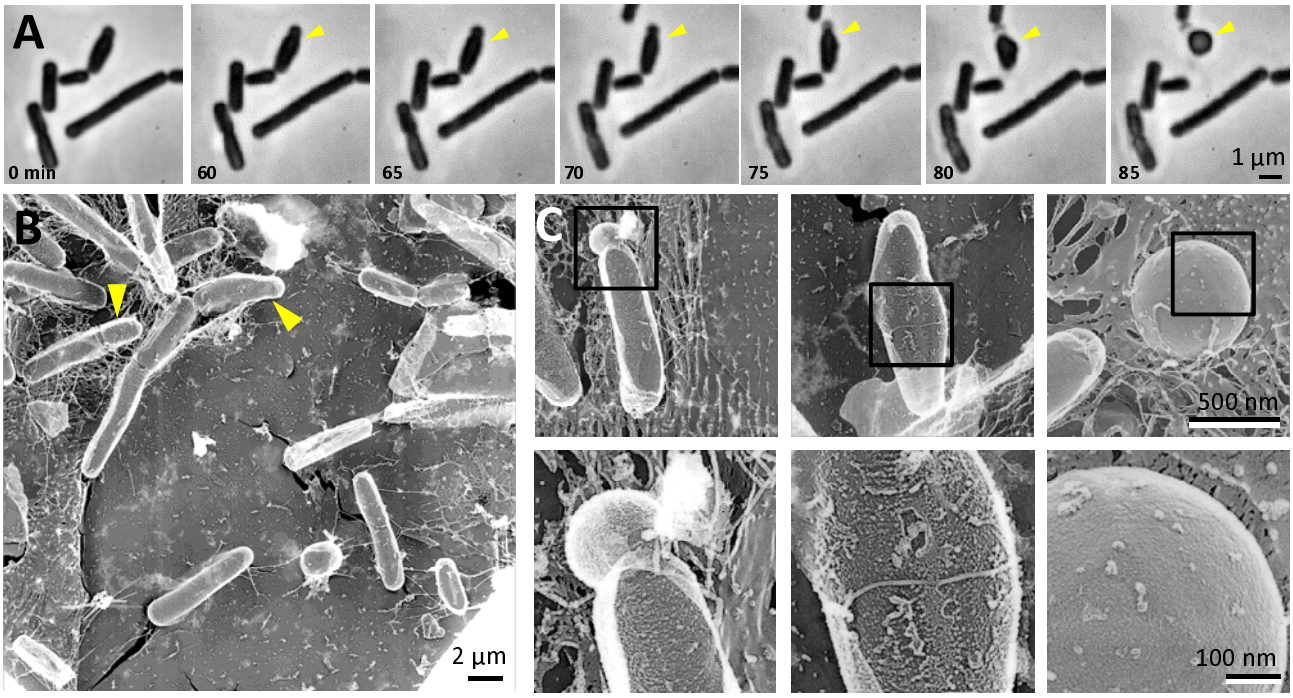

Fig. 4. Effects on cell structure by *murE* operon repression. **A)** Phase-contrast microscopic images taken at 5-minutes intervals at 60 minutes after repression. The cell marked by a yellow triangle changed its structure drastically. A tapered polar, a bulge, and swollen cells can be observed sequentially with time on the cell. **B, C)** Quick-freeze, deep-etch EM images of cells repressed for *murE* for 85 minutes. **C**) Cell features resulted by *murE* repression. The area boxed in the upper panels are magnified in the lower panels.

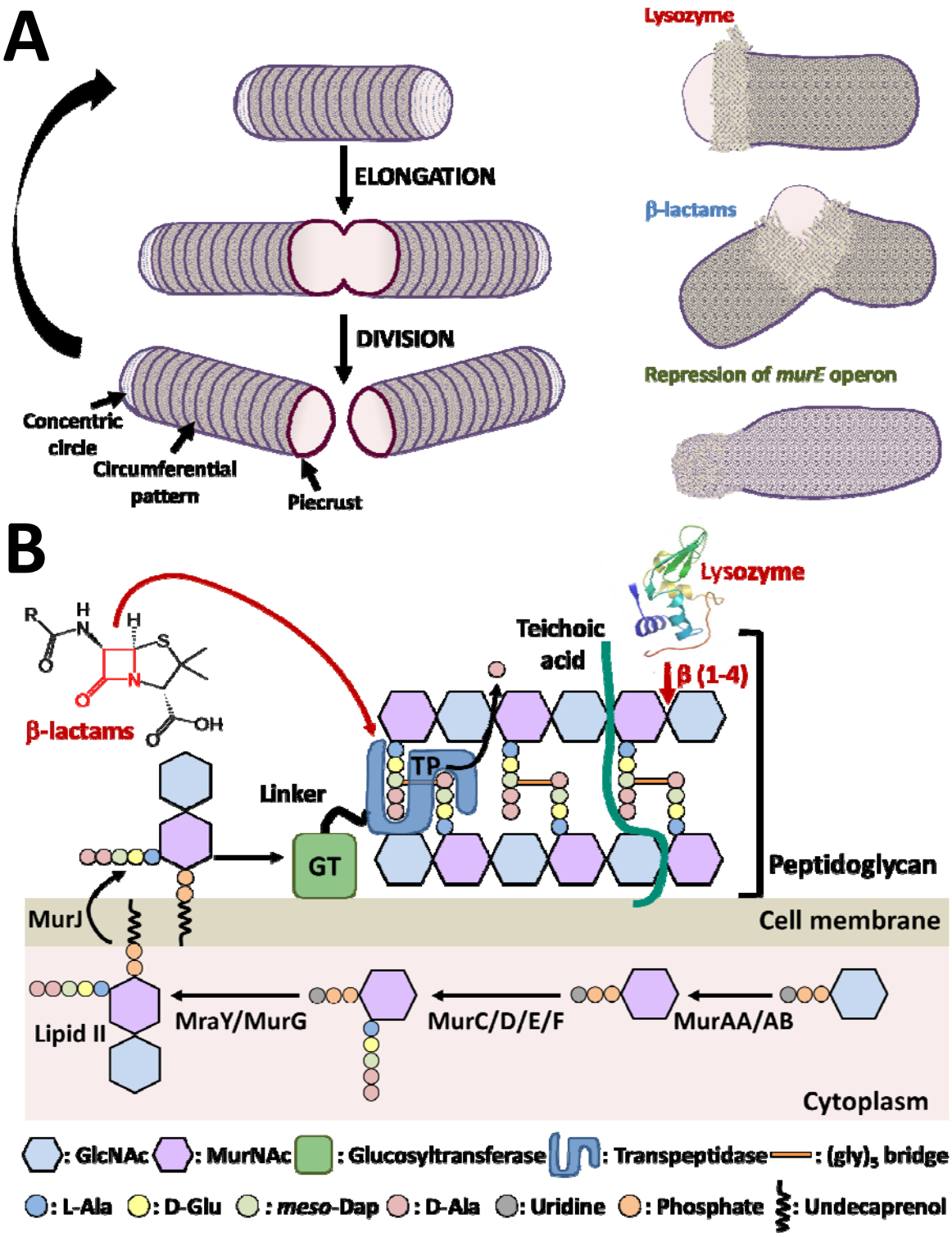

Fig. 5. Schematic presentations of peptidoglycan architecture and working points of inhibitory factors. **A)** Structural features on surfaces of cells in division cycle (left) and peptidoglycan disruption (right). **B)** Chemical processes. The peptidoglycan layer consists of strands of repeating GlcNAc and *N*-acetylmuramic acid MurNAc subunits. Transpeptidase (TP) forms a crosslink between two sugar chains by forming peptidoglycan network. Glycosyltransferase forms linkages between GlcNAc and MurNAc residues. Peptidoglycan synthesis starts in the cytoplasm, where the nucleotide precursors are synthesized by the Mur enzymes (MurA, MurB, MurC, MurD, MurE and MurF). A GlcNAc moiety is transferred by MurG, linked to the undecaprenyl phosphate (transport lipid I), resulting in anchoring to the cell membrane. The antibiotic beta-lactams represented by PenG bind to and inhibit the activity of the transpeptidase by forming a highly stable penicilloyl-enzyme intermediate. Lysozyme cleaves the bond between MurNAc and the fourth carbon atom of GlcNAc. The depletion of MurE blocks the supply of muropeptides.

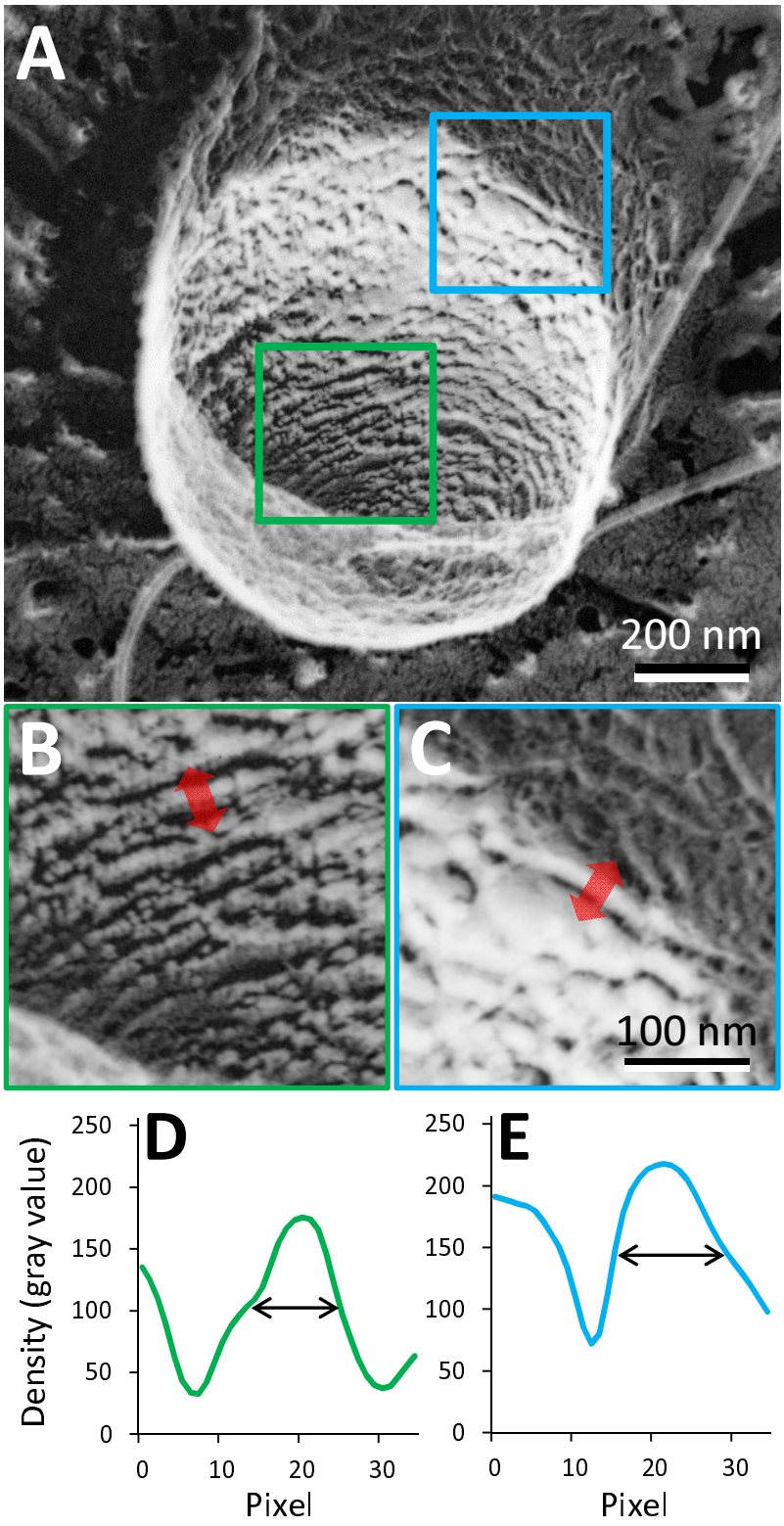

Fig. S1. Measurement of filament width. A) Cell surface image by quick-freeze, deep-etch EM. B, C) Magnified image of areas marked by colored box in panel (A). D, E) Image profiles of red arrow area in panels (B) and (C). The positions at the mid density was defined as the boundary of focusing filament.